J Physiol 594.7 (2016) pp 1891–1910

JPn Neuroscience The Journal of Physiology

Primary visual cortex shows laminar-specific and balanced circuit organization of excitatory and inhibitory synaptic connectivity

Xiangmin Xu[1,2], Nicholas D. Olivas[1,6], Taruna Ikrar[1], Tao Peng[3,4], Todd C. Holmes[5], Qing Nie[2,3,4] and Yulin Shi[1]

[1]*Department of Anatomy and Neurobiology, School of Medicine*
[2]*Department of Biomedical Engineering*
[3]*Department of Mathematics*
[4]*Center for Complex Biological Systems*
[5]*Department of Physiology and Biophysics, School of Medicine, University of California, Irvine, CA, USA*
[6]*Present address: Department of Neurobiology, David Geffen School of Medicine, University of California, Los Angeles, CA, USA*

Key points

- Using functional mapping assays, we conducted a quantitative assessment of both excitatory and inhibitory synaptic laminar connections to excitatory neurons in layers 2/3–6 of the mouse visual cortex (V1).
- Laminar-specific synaptic wiring diagrams of excitatory neurons were constructed on the basis of circuit mapping.
- The present study reveals that that excitatory and inhibitory synaptic connectivity is spatially balanced across excitatory neuronal networks in V1.

Abstract In the mammalian neocortex, excitatory neurons provide excitation in both columnar and laminar dimensions, which is modulated further by inhibitory neurons. However, our understanding of intracortical excitatory and inhibitory synaptic inputs in relation to principal excitatory neurons remains incomplete, and it is unclear how local excitatory and inhibitory synaptic connections to excitatory neurons are spatially organized on a layer-by-layer basis. In the present study, we combined whole cell recordings with laser scanning photostimulation via glutamate uncaging to map excitatory and inhibitory synaptic inputs to single excitatory neurons throughout cortical layers 2/3–6 in the mouse primary visual cortex (V1). We find that synaptic input sources of excitatory neurons span the radial columns of laminar microcircuits, and excitatory neurons in different V1 laminae exhibit distinct patterns of layer-specific organization of excitatory inputs. Remarkably, the spatial extent of inhibitory inputs of excitatory neurons for a given layer closely mirrors that of their excitatory input sources, indicating that excitatory and inhibitory synaptic connectivity is spatially balanced across excitatory neuronal networks. Strong interlaminar inhibitory inputs are found, particularly for excitatory neurons in layers 2/3 and 5. This differs from earlier studies reporting that inhibitory cortical connections to excitatory neurons are generally localized within the same cortical layer. On the basis of the functional mapping assays, we conducted a quantitative assessment of both excitatory and inhibitory synaptic laminar connections to excitatory cells at single cell resolution, establishing precise layer-by-layer synaptic wiring diagrams of excitatory neurons in the visual cortex.

(Resubmitted 11 November 2015; accepted after revision 27 January 2016; first published online 4 February 2016)
Corresponding author X. Xu: Department of Anatomy and Neurobiology, School of Medicine, University of California, Irvine, CA 92697-1275, USA. Email: xiangmin.xu@uci.edu

Abbreviations aCSF, artificial cerebrospinal fluid; DAPI, 4′-6-diamidino-2-phenylindole; LSPS, laser scanning photostimulation; V1, primary visual cortex.

DOI: 10.1113/JP271891

Introduction

The primary visual cortex (V1), similar to other cortical areas, contains excitatory and inhibitory cell types (Markram *et al.* 2004; Xu *et al.* 2010*a*). Excitatory neurons are a principal cell group; they account for ∼80% of the whole cortical neuronal population and convey cortical excitation in both laminar and columnar dimensions. Given that cortical information processing is regulated by diverse types of inhibitory neurons (∼20% of the cortical neurons) and largely determined by local excitatory and inhibitory circuit interactions (Hasenstaub *et al.* 2005; Ikrar *et al.* 2012; Haider *et al.* 2013; D'Amour J & Froemke, 2015), understanding how cortical circuits operate requires the clarification of both excitatory and inhibitory circuit connectivity. Although laminar organization of cortical circuits and the flow of cortical excitation in V1 have been established using anatomical and physiological methods (Callaway, 1998; Douglas & Martin, 2004; Olivas *et al.* 2012), constructing layer-specific connectivity in cortical circuits based on identified neuronal types and their synaptic connections is much more difficult. Excitatory circuit connections to excitatory neurons in different V1 layers have been studied *in vitro* using physiological approaches such as paired intracellular recordings of synaptically connected neurons (Thomson & Lamy, 2007) and laser scanning photostimulation (LSPS) in which wider input sources are mapped to intracelluarly recorded neurons (Dantzker & Callaway, 2000; Yoshimura *et al.* 2005; Zarrinpar & Callaway, 2006). The data derived have added important information on local functional circuit connections. However, the knowledge of intracortical synaptic connections to principal excitatory neurons in V1 still remains incomplete because most studies focus on excitatory neurons in a single cortical layer and there has yet to be a comprehensive and quantitative analysis that examines and compares excitatory synaptic connections to excitatory cell types across cortical layers 2/3–6. In addition, few studies have examined local laminar inhibitory connections to excitatory neurons in the sensory cortex (Xu & Callaway, 2009; Katzel *et al.* 2010) and it remains unclear how their excitatory and inhibitory synaptic connections are spatially arranged on a layer-by-layer basis across local cortical circuitry. Although excitatory cells receive dense inhibitory neuronal innervation in highly localized microcircuits (Fino & Yuste, 2011; Packer & Yuste, 2011), recent work suggests significant interlaminar or cross-laminar inhibitory connections to excitatory neurons (Kapfer *et al.* 2007; Silberberg & Markram, 2007; Apicella *et al.* 2012; Olsen *et al.* 2012; Harris & Shepherd, 2015; Pluta *et al.* 2015), prompting inhibitory cortical connections to be examined systematically using circuit mapping approaches.

In the present study, we used LSPS combined with whole cell recordings (Xu & Callaway, 2009; Ikrar *et al.* 2011; Kuhlman *et al.* 2013) to characterize and compare local circuit connectivity of the excitatory neurons in layers 2/3–6 in living mouse V1 slice preparations. We provide a quantitative assessment of the spatial distribution and input strength of excitatory and inhibitory connectivity with respect to individual pyramidal neurons across V1 laminar circuits, and construct laminar-specific synaptic wiring diagrams of excitatory neurons. The present study provides new knowledge on inhibitory laminar circuit connections and indicates that excitatory and inhibitory synaptic connectivity is spatially balanced onto V1 excitatory neurons.

Methods

Visual cortical slice preparations

C57/B6 strain mice including C57/B6 back-crossed GIN (Oliva *et al.* 2000) and G42 mice (Chattopadhyaya *et al.* 2004) from either sex were used for the experiments, in which one animal yielded one or two high-quality V1 slices with clear laminar and cytoarchitectonic features. The GIN and G42 mice express green fluorescent protein in subsets of inhibitory cortical neurons, which facilitated targeted recordings of inhibitory neurons for calibration experiments. All animals were handled and the experiments conducted in accordance with procedures approved by the Institutional Animal Care and Use Committee at the University of California, Irvine. To prepare living brain slices, animals (postnatal days 17–21) were deeply anaesthetized with Nembutal (>100 mg kg^{-1}, I.P.), rapidly decapitated and their brains removed. The occipital lobe was dissected, and 400 μm thick visual cortical sections were cut in the coronal but slightly oblique plane (∼75° relative to the transverse) (Fig. 1) with a vibratome (VT1200S; Leica Microsystems, Wetzlar, Germany) in sucrose-containing artificial cerebrospinal fluid (aCSF) (in mM): 85 NaCl, 75 sucrose, 2.5 KCl, 25 glucose, 1.25 NaH_2PO_4, 4 $MgCl_2$, 0.5 $CaCl_2$ and 24 $NaHCO_3$. This slice preparation preserves cell morphology and intracortical connections (Fig. 3). Slices were incubated for at least 30 min in sucrose containing aCSF at 32°C before being transferred into slice recording chambers with normal aCSF (in mM): 126 NaCl, 2.5 KCl, 26 $NaHCO_3$, 2 $CaCl_2$, 2 $MgCl_2$, 1.25 NaH_2PO_4 and 10 glucose. Throughout the cutting, incubation and recording, solutions were continuously supplied with 95% O_2/5% CO_2. All steps were taken to use only healthy responsive slices. For a specific cut-off time, recordings were made within 5 h after the slice cutting.

Electrophysiology and LSPS

Our overall system of electrophysiological recordings, imaging and photostimulation was described in detail previously (Xu *et al.* 2010*b*). Slices were first placed

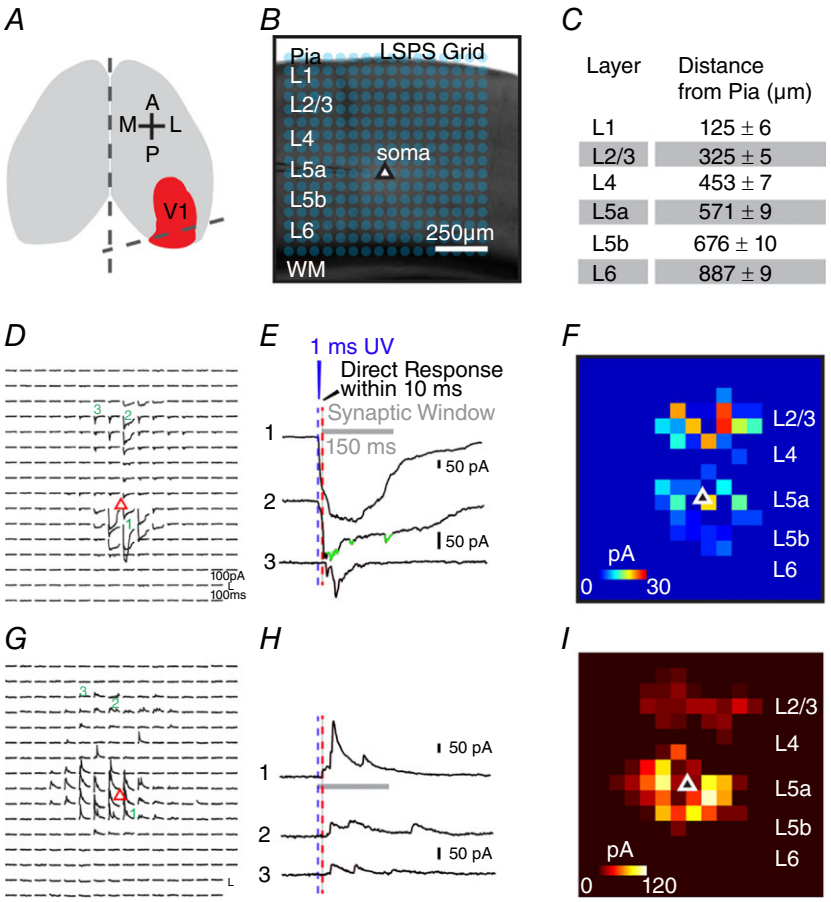

Figure 1. V1 slice preparation and LSPS circuit mapping
A, schematic V1 slice preparation: slices are made from mouse primary visual cortex, cut at a 75° oblique angle relative to midline to preserve intracortical laminar connections. *B*, illustration of LSPS mapping of local cortical circuit input to single recorded cells. Excitatory neurons are recorded from binocular V1 region in whole cell mode, and the slice image is superimposed with a 16 × 16 LSPS mapping grid (blue dots, 65 μm^2 spacing) centred around the cell soma (triangle) and is aligned to the pial surface. Laminar boundaries are determined by cytoarchitectonic landmarks in bright-field slice images, validated by the boundaries determined by *post hoc* DAPI staining. *C*, average depth of laminar boundaries measured from the pial surface to the bottom edge of each layer ($n = 15$ slices). *D*, representative LSPS excitatory input map from voltage clamping an L5a pyramidal neuron at −70 mV in response to spatially restricted glutamate uncaging in the mapping grid (*B*). Each trace is plotted at the LSPS location shown in (*B*). *E*, detailed view of evoked EPSCs measured from the L5a pyramidal neuron at three respective locations numbered in (*D*). Trace 1 demonstrates a large 'direct response' resulting from uncaging at the perisomatic region. Trace 2 provides an example of a relatively small direct response in L2/3 from uncaging at the apical dendrite coupled with overriding synaptic inputs (shown in green). Trace 3 illustrates synaptic inputs (EPSCs) measured from a L2/3 location. Note the difference of amplitudes and latencies of direct and synaptic input responses, thus allowing for functional characterization. Empirically, responses within the 10 ms window from laser onset are considered direct, and exhibit a distinct shape (shorter rise time) and occurred immediately after glutamate uncaging (shorter latency). Synaptic events (i.e. EPSCs) are measured with the analysis window of >10–160 ms after photostimulation (grey bar). For details, see Methods. *F*, colour-coded EPSC input map showing the overall spatial distribution and strength of excitatory inputs to the recorded L5a pyramidal cell. The map is constructed from the responses shown in (*D*); input responses per location are quantified in terms of average integrated EPSC strength within the analysis window, and colour coded according to the amplitude. *G*, representative LSPS inhibitory input map from voltage clamping an L5a pyramidal neuron at 5 mV in response to LSPS in the mapping grid similar to (*D*). *H*, examples of evoked IPSCs measured in an L5a pyramidal neuron at three respective locations numbered in (*G*). Trace 1 demonstrates large IPSCs measured near the cell soma. Traces 2 and 3 provide examples of interlaminar inhibition from L2/3. Consistent with excitatory inputs, IPSCs were measured with the analysis window of >10–150 ms after photostimulation (grey bar). *I*, colour-coded IPSC input map showing the overall spatial distribution and strength of inhibitory inputs made to the L5a pyramidal cell.

Table 1. Electrophysiological properties of V1 excitatory neurons

	L2/3	L4	L5a	L5b	L6
AP threshold (mV)	–40 ± 3.4	–36 ± 3	–36.2 ± 5.9	–36.9 ± 5.6	–31 ± 1.7
AP ht (mV)	73.8 ± 3.1	68 ± 1.8	78.9 ± 3.3	72.9 ± 3.3	66.6 ± 3.4
AP hw (ms)	2.9 ± 0.2	2.3 ± 0.1	2.2 ± 0.3	2.8 ± 0.5	2.1 ± 0.2
AHP (mV)	11.3 ± 0.9	11.1 ± 1	10.3 ± 2.1	12.1 ± 1.7	11.4 ± 1
AHP time (ms)	27.1 ± 2.8	22.4 ± 1.8	30 ± 0.01	26.7 ± 2.7	15.8 ± 2.5
AP rise time (ms)	1.2 ± 0.2	1 ± 0.04	0.9 ± 0.1	1 ± 0.1	1.1 ± 0.1
AP fall time (ms)	5.2 ± 0.4	4 ± 0.2	4.9 ± 0.7	5.4 ± 1	3.4 ± 0.3
Initial ISI (s)	0.04 ± 0.02	0.02 ± 0.004	0.04 ± 0.01	0.03 ± 0.001	0.03 ± 0.004
Spike rate (Hz)	15 ± 1.1	23 ± 1.8	19.2 ± 3	26.5 ± 10	22.1 ± 1.8
Spike adaptation index	4 ± 0.4	4 ± 0.3	4.6 ± 1	4.2 ± 0.4	3. 7 ± 0.6

The intrinsic physiological characteristics of individual pyramidal neurons recorded across V1 layers were quantitatively measured and grouped according to laminar location (L2/3–L6). Included in the measurements are action potential (AP) threshold, height (ht), half-width (hw), after hyperpolarization potential (AHP) and duration (AHP time), AP rise and fall time, the initial interspike interval (ISI) and spike rate at 200 pA of somatic current injection (Hz), and spike adaptation index. Data are presented as the mean ± SE.

and carefully examined under a 4× objective of a DIC/fluorescence microscope (BX51WI; Olympus, Tokyo, Japan) for proper laminar targeting of excitatory neurons within binocular regions of mouse V1 using the landmarks defined in Antonini *et al.* (1999). To perform whole cell recordings, neurons were visualized at high magnification (60× objective, 0.9 NA; LUMPlanFl/IR; Olympus). Cell bodies of recorded neurons were at least 50 μm below the slice cutting surface and were initially targeted based upon the pyramidal appearance of the cell soma and thick apical dendrite when possible. Patch pipettes (4–6 MΩ resistance) made of borosilicate glass were filled with an internal solution, containing (in mM) 126 K-gluconate, 4 KCl, 10 Hepes, 4 ATP-Mg, 0.3 GTP-Na and 10 phosphocreatine (pH 7.2; 300 mOsm), for examination of intrinsic electrophysiology in current clamp mode and measurement of EPSCs with the membrane potential voltage clamped at −70 mV. In separate recordings, potassium was replaced with caesium in the internal solution; the caesium-based internal solution, containing (in mM): 130 CsOH, 130 D-gluconic acid, 0.2 EGTA, 2 $MgCl_2$, 6 CsCl, 10 Hepes, 2.5 ATP-Na, 0.5 GTP-Na and 10 phosphocreatine (pH 7.2; 300 mOsm), was used to hold excitatory neurons at membrane potentials (0–5 mV) in voltage clamp mode and measure IPSCs. The internal solutions also contained 0.1% biocytin for *post hoc* cell labelling and further morphological identification. Once stable whole-cell recordings were achieved with good access resistance, basic electrophysiological properties were examined through hyperpolarizing and depolarizing current injections. Spike frequency and adaptation and spike shape analysis (Table 1) were conducted as described previously (Xu *et al.* 2006). Electrophysiological data were acquired with a Multiclamp 700B amplifier (Molecular Devices, Sunnyvale, CA, USA), data acquisition boards (models PCI MIO 16E-4 and 6713; National Instruments, Austin, TX, USA) and a modified version of Ephus, version 5 (https://openwiki.janelia.org). Data were digitized at 10 kHz and stored on a PC. Only neurons with an initial resting membrane potentials more negative than −55 mV and stable input resistances of <30 MΩ were used. Any recordings in which the access resistance changed by >20% during the course of the experiment were excluded from analysis.

During photostimulation experiments, the microscope objective was switched from 60× to 4× for delivery of the UV flash stimuli. A stock solution of MNI-caged-L-glutamate (Tocris Bioscience, St Louis, MO, USA) was added to 20 ml of circulating aCSF for a concentration of 0.2 mM caged glutamate. The cortical slice image was acquired at the 4× objective by a high-resolution digital CCD camera, which in turn was used for guiding and registering photostimulation sites. A laser unit (DPSS Lasers, Santa Clara, CA, USA) was used to generate 355 nm UV laser pulses for glutamate uncaging. Short pulses of laser flashes (1 ms, 15 mW) were controlled using an electro-optical modulator and a mechanical shutter. The laser beam formed uncaging spots, each approximating a Gaussian profile with a width of 50-100 μm laterally at the focal plane. Physiologically, under our experimental conditions, LSPS-evoked action potentials (APs) only occurred from stimulation locations within ∼100 μm of targeted somata and occurred within ∼10–150 ms after photostimulation. During the experiments mapping photostimulation-evoked spiking profiles (excitability profiles), individual excitatory neurons and inhibitory interneurons were recorded in whole cell mode and the spatial distribution of LSPS-evoked APs was measured relative to the cell soma. Our data show that, under our experimental conditions, LSPS had a sufficient resolution for V1 laminar circuit mapping (see below).

For our mapping experiments, a standard stimulus grid (16 × 16 stimulation sites, 65 μm^2 spacing) was used to cover the V1 slices, spanning from pia to white matter. The LSPS site spacing was empirically determined to capture the smallest predicted distance in which photostimulation differentially activates adjacent neurons, and glutamate uncaging was delivered sequentially in a non-raster, non-random sequence, following a 'shifting-X' pattern designed to avoid revisiting the vicinity of recently stimulated sites (Shepherd & Svoboda, 2005).

Because glutamate uncaging agnostically activates both excitatory and inhibitory neurons, we empirically determined the excitatory and inhibitory reversal potentials in excitatory pyramidal cells to properly isolate EPSCs and IPSCs. During calibration experiments, excitatory neurons were voltage clamped at a range of holding potentials from −90 mV to −50 mV and GABA uncaging (6-cyano-7-nitroquinoxaline-2,3-dione caged GABA, 0.1 mM; Invitrogen, Carlsbad, CA, USA) was performed by delivering brief UV flashes (1 ms, 20 mW) to the perisomatic regions of recorded cells to determine the GABAergic reversal potential. The average GABAergic reversal potential ranged from −69 mV to −71 mV ($n = 5$ excitatory neurons) and so we voltage clamped the targeted pyramidal cells at −70 mV to detect EPSCs. Similarly, the holding potential (0–5 mV) for IPSC detection was determined using glutamate uncaging at a range of holding potentials (−20 mV to +10 mV) with the caesium-containing internal solution.

Laminar circuit input analysis

Photostimulation can induce two major forms of uncaging responses: (1) direct glutamate uncaging responses (direct activation of the glutamate receptors of the recorded neuron) and (2) synaptically mediated responses (either EPSCs or IPSCs) resulting from the suprathreshold activation of presynaptic neurons. Uncaging responses within the 10 ms window from laser onset were considered direct, exhibited a distinct shape often with large amplitudes and occurred immediately after glutamate uncaging, as demonstrated in Fig. 1. Synaptic currents with such short latencies are not possible because they would have to occur before the generation of APs in photostimulated neurons. Therefore, direct responses need to be excluded from the synaptic input analysis. However, at some locations, synaptic responses were overriding on the relatively small direct responses and were identified and included in synaptic input analysis (Fig. 1). For data map analysis, we implemented a new approach for the detection and extraction of photostimulation-evoked postsynaptic current responses (Shi *et al.* 2010), which allows detailed quantitative analyses of both EPSCs and IPSCs (amplitudes and the numbers of events across LSPS stimulation sites). LSPS-evoked EPSCs and IPSCs were first quantified across the 16 × 16 mapping grid for each map and two to four individual maps were averaged per recorded cell, reducing the effect of spontaneous synaptic events. The analysis window (>10 ms to 160 ms) after photostimulation was chosen because photostimulated neurons fired most of their APs during this time (Fig. 2). Averaged maps were analysed and response measurements were assigned to individual laminar locations according to slice cytoarchitectonic landmarks and cortical depths from the pia surface (see below). Laminar distributions, average integrated input strength and the numbers of EPSCs measured in excitatory neurons were quantified. Input maps were plotted with average integrated EPSC or IPSC amplitudes, as well as evoked EPSC and IPSC numbers per location.

Because almost all layer 1 neurons are inhibitory cells, and pyramidal neurons with apical dendritic tufts in layer 1 could fire APs when their tufts were stimulated in layer 1 (Dantzker & Callaway, 2000), EPSCs detected after photostimulation in layer 1 were not included in the analyses. However, because layer 1 neurons can provide inhibition to layer 2/3 neurons, we analysed IPSCs detected after photostimulation in layer 1.

Morphological examination and cell-type identification

After physiological assays, brain slices were fixed in 4% paraformaldehyde overnight and then transferred to 30% sucrose solution in PBS. Slices were stained against biocytin with 1:500 Alexa Fluor 488-conjugated streptavidin (Jackson ImmunoResearch, West Grove, PA, USA) to visualize the morphology of the recorded cells. Slices were also stained for 4′-6-diamidino-2-phenylindole (DAPI) (Sigma-Aldrich, St Louis, MO, USA) to identify laminar boundaries. The cell morphology was visualized using a BX 61 (Olympus) epifluorescence microscope and the MetaMorph imaging suite (Molecular Devices). Based upon *in vitro* cytoarchitectonic landmarks observed in living slice images coupled with *post hoc* DAPI staining, the average depths of laminar boundaries for layers 1, 2/3, 4, 5a, 5b and 6 were determined to be 125 ± 6 μm, 325 ± 5 μm, 453 ± 7 μm, 571 ± 9 μm, 676 ± 10 μm and 887 ± 9 μm, respectively, from the pial surface (Fig. 1). Additionally, the somatic distance from pia was measured for each recorded neuron. These measurements enabled proper identification of the laminar locations of recorded cells and characterization of presynaptic input sources.

Computational modelling

We adopted a discrete dynamical model (Christley *et al.* 2009) with the inference of the connectivity among excitatory neurons at four different cortical layers to describe and simulate photostimulation mapped circuit

activities. The input data of the model were derived from the temporal data based on the LSPS-mapped synaptic inputs (EPSCs and IPSCs) to the representative excitatory neurons in different cortical layers. We extracted the temporal data from LSPS-mapped synaptic inputs to excitatory neurons, with six representative neurons from layer 2/3, four neurons from layer 4, seven neurons from layer 5 and four neurons from layer 6. The integration data of synaptic inputs was extracted at each 10 ms window using the detection method described above. To set a cut-off threshold for background noises, the data points (10 ms per point) with their strengths less than

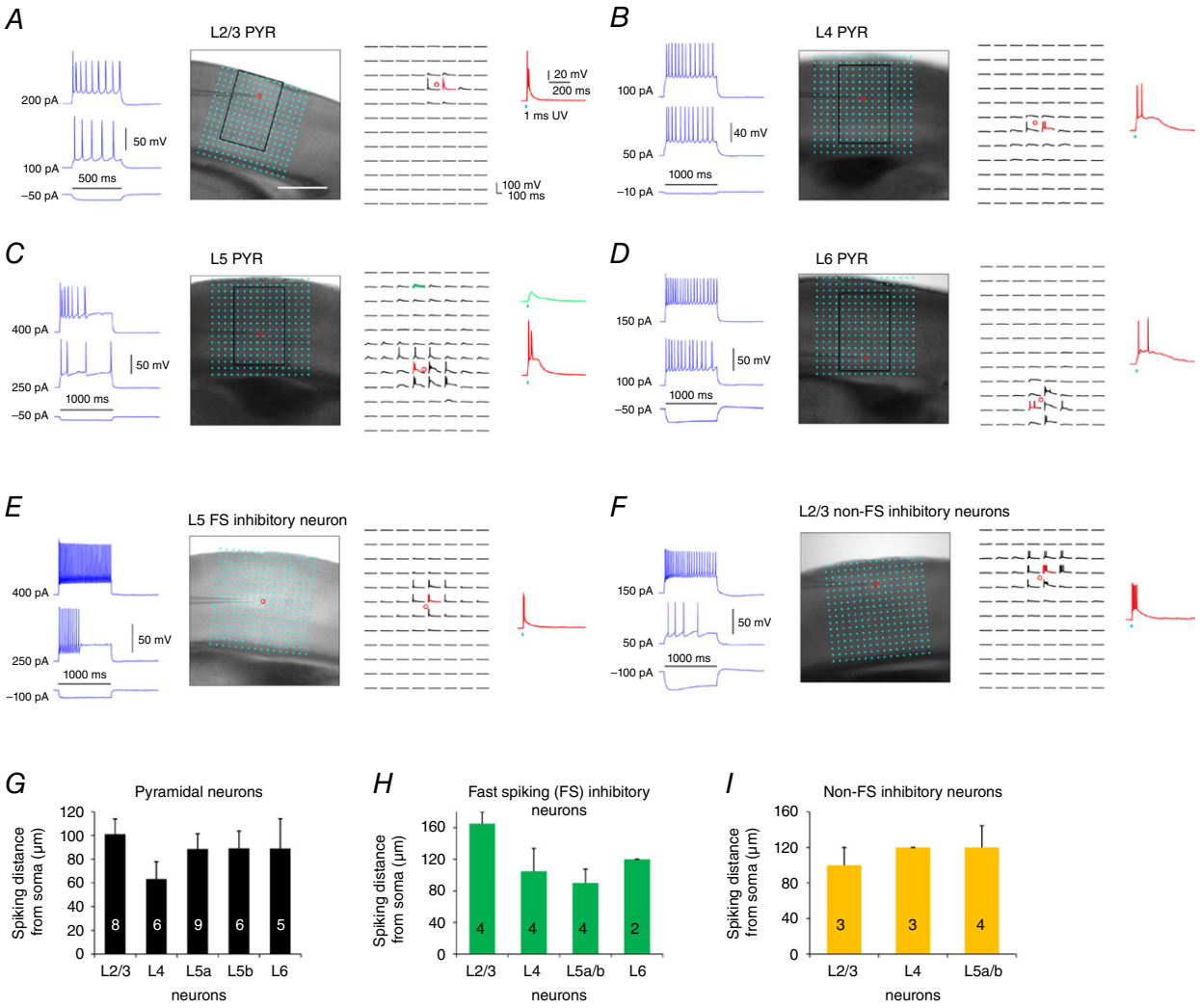

Figure 2. Spatial resolution of photostimulation
A–F, examples of photostimulation-evoked excitability profiles of pyramidal and inhibitory interneurons in different visual cortical layers. *A*, current injection responses of an example L2/3 pyramidal neuron are shown on the left; the image of V1 slice where the cell was recorded in layer 2/3 is superimposed with photostimulation sites (*, cyan dots, 65 μm^2 spacing) (middle) and the photostimulation responses of the recorded neuron are plotted at the beginning of stimulation onset (right). The individual responses are plotted relative to their spatial locations in the mapping array shown in the middle. The small red circle indicates the somatic location of the recorded neuron. One response trace with photostimulation-evoked APs is indicated in red, and shown separately by the side. Laser flashes (1 ms, 15 mW) were applied for photostimulation mapping. The scale in (*A*) is 500 μm. *B–F*, similarly formatted as in (*A*), with example L4, L5 and L6 pyramidal neurons, and L5 fast spiking inhibitory neurons and L2/3 non-fast spiking inhibitory neurons, respectively. *C*, two response traces with photostimulation-evoked subthreshold depolarization (green, photostimulation at the apical dendrite) and suprathreshold APs (red, perisomatic region) are shown separately. *G–I*, spatial resolution of LSPS evoked excitability of pyramidal neurons, fast-spiking and non-fast spiking inhibitory neurons was determined by measuring the LSPS evoked spike distance relative to soma location. Note that the spiking distance is measured as the 'vertical' distance (perpendicular to cortical layers) above and below the cell body. The numbers of recorded neurons are shown at the bar graphs. Data are presented as the mean ± SE.

50 pA/10 ms were set to zero. For photostimulation in each and specific cortical layer (i.e. L2/3, L4, L5 and L6), the overall activation strength was calculated by summing the area under each curve of temporal input evolution across all layers, and the relative laminar activation was obtained by comparing its area under the curve with the overall activation across layers.

Our model consists of the four cortical layers (L2/3, L4, L5 and L6) of excitatory neurons. In this model, a matrix, $W = (W_{ij})_{n,n}$ is used to represent the connectivity strength among different cortical layers. If $W_{ij} > 0$, layer j receives excitatory input from layer i. If $W_{ij} < 0$, layer j receives inhibitory input from layer i. If $W_{ij} = 0$, there is no direct connection between layers i and j. Specifically, for the present study, the $W = (W_{ij})_{4,4}$ has 16 entries, and the entries for L2/3 with L2/3, L4, L5 and L6 are W_{11}, W_{12}, W_{13} and W_{14}. The entries for L4 with L2/3, L4, L5 and L6 are W_{21}, W_{22}, W_{23} and W_{24}. The entries for L5 with L2/3, L4, L5 and L6 are W_{31}, W_{32}, W_{33} and W_{34}. The entries for L6 with L2/3, L4, L5 and L6 are W_{41}, W_{42}, W_{43} and W_{44}. The data from the mapping experiment were then used to fit the linear system to solve for W. The data fitting is further constrained by including the prior knowledge of the connectivity of cortical layers, as well as a term that controls the density of the connections, which may potentially remove very weak interlaminar connections. The model provides an optimal estimate for the connectivity strength matrix by minimizing the difference between the model-calculated signals and the measured experimental signals. Such an approach has been successfully used to obtain the gene regulatory network based on gene expression data (Christley *et al.* 2009).

Mathematically, the objective function for fitting the model to the data is:

$$W^* = \arg\min_W (g(W) + \alpha||W||_1 + \beta||W \circ W^0||_1)$$

where

$$g(W) = \sum_{h=1}^{p}\sum_{k=1}^{n}\sum_{l=1}^{m} ||W{x_l}^{k,h} - {u_l}^{k,h}||_2^2.$$

In the objective function, α and β are the non-negative numbers and W^0 is the prior knowledge of the connectivity strength of cortical layers (i.e. laminar relative activation; see above). The m (= 4) is the number of the given laminar photostimulation, the n (= 15) is the number of data pairs at each given photostimulation, the p (= 2) is the number of types of synaptic inputs (excitation and inhibition). If there is a connection from layer i to layer j, $w_{ij}^0 = 0$; otherwise, $w_{ij}^0 = 1$. $||W||_1$ is the term for controlling the sparseness of the network (i.e. the density of the connections), and $||W \circ W^0||_1$ is for incorporating the prior information where $\circ$ is the operation for the entry-wise multiplication. In the model, we used a simplified version of the network map as the prior information. The measured experimental data input, ${x_l}^{k,h}$, represents input strengths of L2/3, L4, L5 and L6 at time point k with a lth layer photostimulation ($l = 1, 2, \ldots, 4$; photostimulation in L2/3, L4, L5 or L6), given hth type laminar photostimulation (for measuring excitation or inhibition), and ${u_l}^{k,h}$ represents input strengths of L2/3, L4, L5 or L6 at time point $k+1$ at the lth layer photostimulation given hth type laminar photostimulation as the corresponding output of ${x_l}^{k,h}$. $W{x_l}^{k,h}$ is the model-calculated input strengths of L2/3, L4, L5 or L6 at time point $k+1$ at the lth given hth type laminar photostimulation. The objective of the modelling is to obtain the optimal connectivity strength matrix W^* by minimizing the difference between the model-calculated input strengths $W{x_l}^{k,h}$ and the measured experimental input strengths ${u_l}^{k,h}$. For each given laminar photostimulation, there were 16 time points, including 15 data pairs $(x_l^{k,h}, u_l^{k,h})$, where $k = 1, 2, \ldots, 15$, $l = 1, 2, \ldots, 4$ (photostimulation in L2/3, L4, L5 or L6 respectively) and $h = 1, 2$ (measuring excitation or inhibition). Altogether, 120 data pairs ($15 \times 4 \times 2$) were employed to train the model. We used the standard 10-fold cross-validation technique from machine learning to determine the values of α and β. Then, the optimal connectivity matrix W^* was calculated using the algorithm described in our previous study (Christley *et al.* 2009).

Statistical analysis

Data are presented as the mean ± SE. For statistical comparisons between groups, the data were checked for normality distribution and equal variance. If the criteria were met, a t test was performed to compare two groups; when the criteria were not met, a Mann–Whitney U test was used. For statistical comparisons across more than two groups, we used the Kruskal–Wallis test (non-parametric one-way ANOVA) and the Mann–Whitney U test for group comparisons. In all experiments, $P < 0.05$ was considered statistically significant.

Results

LSPS mapping of mouse V1 intracortical synaptic organization

LSPS combined with whole cell recordings has been effectively applied for analysing cortical circuit organization (Schubert *et al.* 2003; Shepherd *et al.* 2003; Shepherd & Svoboda, 2005; Yoshimura *et al.* 2005; Zarrinpar & Callaway, 2006; Weiler *et al.* 2008; Xu & Callaway, 2009; Oviedo *et al.* 2010; Xu *et al.* 2010*b*; Hooks *et al.* 2011; Ikrar *et al.* 2011). It allows for high resolution mapping of presynaptic input sources to single neurons at a local

circuit level, and the simultaneous recording from a postsynaptic neuron with sequential photostimulation of clusters of presynaptic neurons at many different locations provides a quantitative measure of the spatial distribution of excitatory or inhibitory inputs in the broad range of the photostimulation field. As shown in Fig. 1, the LSPS approach involves recording from single neurons, then stimulating at surrounding sites on the LSPS mapping grid to generate APs from neurons in those sites, thus providing a map for the recorded neuron based on activation of presynaptic inputs. With subsequent anatomical characterization of the postsynaptic neuron, as well as its functional properties, the cell type can be classified, allowing a map of input sources to be generated for a known cell type.

To interpret input maps, it is first necessary to determine the spatial extent or precision with which neurons at the stimulation site respond. As shown in Fig. 2, individual excitatory neurons ($n = 34$ across the layers) and inhibitory interneurons (14 fast-spiking inhibitory neurons and 10 non-fast spiking inhibitory neurons) were recorded in whole cell mode and the spatial precision/resolution of photostimulation was assessed by the photostimulation-evoked spiking distance between the recorded neuron and the stimulation site. The distance is expressed as the 'vertical' distance (perpendicular to cortical layers) above and below the cell body because this is the measurement that is relevant for assignment of stimulation sites to correct layers. Recordings of fast spiking inhibitory neurons (Fig. 2*E* and *H*) and non-fast spiking inhibitory neurons (Fig. 2*F* and *I*) were facilitated by identification of EGFP expression in these cell types using G42 and GIN mice (Xu & Callaway, 2009).

Overall, photostimulation-evoked neuronal excitability profiles indicate that LSPS has a sufficient resolution for V1 laminar circuit mapping. The mean ± SE distances of photostimulation-evoked APs from the recorded cell bodies for layer 2/3 (L2/3), layer 4 (L4), layer 5a (L5a), layer 5b (L5b) and layer 6 (L6) pyramidal neurons were 101.3 ± 12.8 μm, 63.3 ± 14.6 μm, 88.6 ± 13 μm, 89.2 ± 14.7 μm and 89 ± 25.2 μm, respectively (Fig. 2*A–D* and *G*). The numbers of APs evoked per spiking location were 1.9 ± 0.2 APs. The spiking distances for fast-spiking and non-fast spiking inhibitory interneurons appeared to be slightly larger than those of excitatory neurons, varying from ∼90 μm to 160 μm in different cortical layers (Fig. 2*E–F* and *H–I*). The average distances of pooled inhibitory neurons were 117.5 ± 8.5 μm, and the numbers of evoked spikes measured per spiking location were 2.2 ± 0.5 APs. These excitability profiles further indicate that photostimulation-evoked spiking occurs upon direct stimulation and not through excitation of synaptically coupled neurons. Note that we could have restricted analyses to stimulation sites at least 65 μm from the laminar boundaries to further reduce ambiguity in determining laminar locations of presynaptic neurons (e.g. L4 *vs.* L5a, or L5b *vs.* L6), although our preliminary measurements showed no significant differences in the quantification of the laminar input patterns of cells compared to those not excluding the sites at laminar boundaries. Taken together, these data validate the use of LSPS for laminar circuit mapping of direct excitatory and inhibitory synaptic connections to V1 excitatory neurons.

We recorded from 66 excitatory neurons ($N = 14, 15, 10, 11$ and 16 cells for L2/3, L4, L5a, L5b and L6, respectively) that were morphologically and physiologically identified as excitatory pyramidal neurons (Fig. 3), and their excitatory synaptic connections from local circuits were assayed quantitatively. In terms of intrinsic electrophysiology, these excitatory cells exhibited relatively uniform properties associated with spike frequency and adaptation and spike shapes in response to intrasomatic current injection (Table 1). In addition, another 57 excitatory neurons ($n = 10$, 17, 10, 10 and 10 cells for L2/3, L4, L5a, L5b and L6, respectively) were separately recorded to map inhibitory synaptic connections in local V1 circuits.

Laminar excitatory inputs to V1 excitatory cells

Excitatory neurons in different V1 laminae exhibit distinct patterns of laminar-specific organization of excitatory inputs (Fig. 4). Neurons were binned according to their laminar location and the aggregate synaptic input maps are

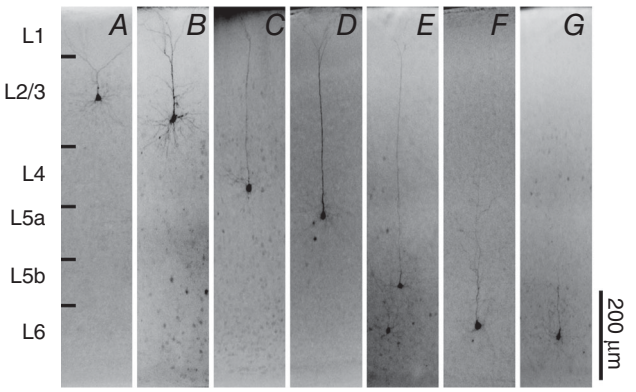

Figure 3. Morphological profiles of V1 excitatory neurons
Neurons recorded for laminar synaptic input analyses were morphologically examined via biocytin staining. DAPI counterstain was used to establish layer identity. *A*, representative upper L2/3 pyramidal neuron with truncated apical dendrites. *B*, excitatory neurons in deeper L2/3 exhibiting longer apical dendrites projecting toward the pial surface. *C*, almost all L4 excitatory cells recorded confirmed pyramidal cells with apical dendrites projecting toward the pial surface. *D–E*, L5a and L5b excitatory cells exhibiting typical tall pyramidal cell morphology. *F*, long L6 pyramidal cell with apical dendrites projecting into L5 and L4. *G*, example of a L6 pyramidal neuron with short apical dendrites terminating in L5.

displayed as averaged maps corresponding to postsynaptic locations of recorded excitatory cells.

L2/3 pyramidal neurons receive the strongest excitatory input from L4 and L5a, weaker excitatory inputs from L2/3 and L5b, and minimal input from L6 (Fig. 4*A* and *C* and Table 2). We also normalized laminar input strength as the percentage evoked input by expressing the average evoked input from each layer as a percentage of the summed input from all layers (Table 2) (Xu & Callaway, 2009). The numbers of LSPS-evoked EPSCs per location are also

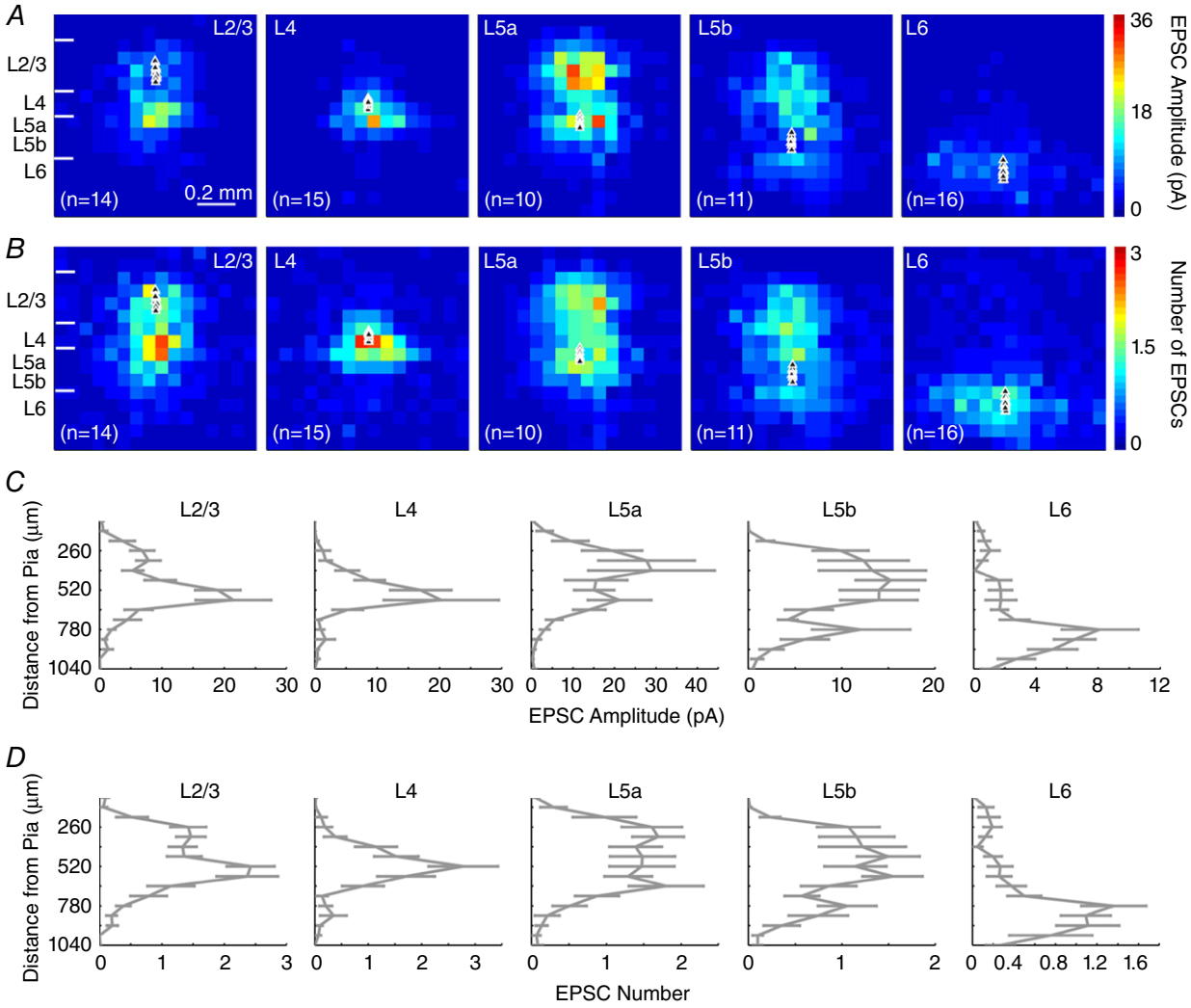

Figure 4. Local excitatory inputs to V1 pyramidal neurons
A, group averaged excitatory input maps for excitatory pyramidal cells for each cortical lamina (L2/3, L4, L5a, L5b and L6). Each colour coded pixel represents the average evoked EPSC amplitude across the LSPS mapping grid; white triangles represent the cell body locations of recorded pyramidal neurons. The left most map charts laminar V1 boundaries relative to the 16 × 16 mapping grid based on *post hoc* DAPI counterstaining. *B*, numbers of EPSCs per LSPS location are plotted from the averaged maps presented in (*A*). For normalization, colour-coded laminar excitatory input maps are scaled to the highest input value across groups. *C*, EPSC amplitudes are quantified across the radial vector corresponding to the columnar position of recorded cells across layers. *D*, laminar profiles of EPSC numbers are quantified across the radial vector corresponding to the columnar position of recorded cells throughout the cortical depth, similar to (*C*). Data are presented as the mean ± SE. For the L2/3 pyramidal cells examined, the average numbers of evoked EPSCs per photostimulation are 1.1 ± 0.3, 1.8 ± 0.4, 1.5 ± 0.5, 0.5 ± 0.3 and 0.2 ± 0.1 for L2/3, L4, L5a, L5b and L6, respectively. The average numbers of evoked EPSCs per photostimulation for L4 pyramidal neurons are 0.5 ± 0.2, 2.2 ± 0.7 and 1.3 ± 0.5 in L2/3, L4 and L5a, respectively. The average numbers of evoked EPSCs per photostimulation for L5 pyramidal neurons are 1.4 ± 0.2, 1.5 ± 0.8, 1.5 ± 0.7, 0.8 ± 0.1 and 0.3 ± 0.2 from L2/3, L4, L5a, L5b and L6, respectively, whereas L5b cell values are 1.0 ± 0.3, 1.3 ± 0.7, 1.2 ± 0.6, 0.6 ± 0.1 and 0.7 ± 0.2 from L2/3, L4, L5a, L5b and L6, respectively. The average numbers of evoked EPSCs per photostimulation for L6 cells are 0.2 ± 0.6, 0.3 ± 0.5, 0.5 ± 0.1 and 1.1 ± 0.1 for L4, L5a, L5b and L6, respectively.

Table 2. LSPS evoked input (EI) and percentage evoke input (%EI) from each cortical layer to targeted excitatory cells across local V1 circuits

	L2/3 cells		L4 cells		L5a cells		L5b cells		L6 cells	
Input layer	EI (pA)	%EI	EI (pA)	%EI	EI (pA)	%EI	EI (pA)	%EI	EI (pA)	%EI
Excitatory input										
L2/3	5.9 ± 1.9	28.8 ± 9.1	2.1 ± 1.0	13.3 ± 5.6	21.3 ± 9.6	46.4 ± 11.8	9.3 ± 3.6	31.3 ± 11.1	0.6 ± 0.3	5.5 ± 3.0
L4	14.3 ± 3.1	35.4 ± 7.6	12.9 ± 3.7	52.2 ± 10.5	15.3 ± 6.1	18.6 ± 6.0	14.6 ± 3.9	27.6 ± 6.0	1.7 ± 0.7	8.2 ± 4.4
L5a	13.9 ± 4.1	26.7 ± 6.9	12.8 ± 5.8	26.6 ± 7.7	17.6 ± 5.7	22.8 ± 6.8	10.2 ± 3.4	16.6 ± 4.8	1.7 ± 0.8	12 ± 5.0
L5b	4.5 ± 2.1	3.8 ± 1.9	0.58 ± 0.5	1.3 ± 1.0	5.5 ± 2.0	4.1 ± 1.1	4.2 ± 1.0	4.7 ± 4.7	2.6 ± 0.9	6.5 ± 1.6
L6	1.7 ± 0.5	4.6 ± 1.8	1.0 ± 0.7	5.0 ± 3.5	1.7 ± 0.8	4.4 ± 2.1	6.9 ± 3.0	18.5 ± 7.6	6.6 ± 1.7	56.6 ± 12.2
Inhibitory input										
L1	12.3 ± 9.2	5.9 ± 3.7	0.27 ± 0.1	0.6 ± 0.4	0.4 ± 0.2	0.4 ± 0.2	0.4 ± 0.3	0.6 ± 0.5	0.1 ± 0.1	0.2 ± 0.2
L2/3	45.7 ± 11.7	51.8 ± 9.4	8.4 ± 2.4	27.1 ± 7.6	11.8 ± 3.4	19.5 ± 5.0	24.8 ± 13.0	16.9 ± 7.0	0.9 ± 0.5	1.7 ± 1.0
L4	51 ± 11.4	29.0 ± 4.5	35.2 ± 11.5	43.4 ± 9.0	27.5 ± 9.4	21.0 ± 6.3	26.8 ± 9.9	11.7 ± 3.4	6.9 ± 4.6	3.5 ± 2.1
L5a	15.2 ± 3.6	9.55 ± 2.4	14.1 ± 5.1	23.3 ± 6.4	55 ± 10.0	44.0 ± 4.6	39 ± 10.0	19.5 ± 5.4	7.2 ± 3.7	5.0 ± 1.9
L5b	5.2 ± 1.6	1.9 ± 0.7	4.2 ± 2.6	1.6 ± 0.6	24.9 ± 7.6	9.0 ± 2.4	44.8 ± 14.1	11.4 ± 2.2	18.2 ± 5.8	7.3 ± 1.5
L6	1.1 ± 0.4	1.3 ± 0.5	2.0 ± 1.1	3.4 ± 1.6	5.7 ± 2.6	6.0 ± 2.2	51.6 ± 15.0	32.9 ± 8.1	41.3 ± 11.0	79.0 ± 12.8

Excitatory input: laminar excitatory synaptic inputs made onto V1 excitatory cells of layers 2/3 through 6 (columns) mapped by LSPS. Note the absence of excitatory neurons in L1 and hence no excitatory inputs from L1. LSPS evoked inputs are displayed as average excitatory evoked inputs in units of pA from each cortical layer, and the percentage of excitatory evoked input, which shows the relative contribution of synaptic input from each cortical layer to recorded cells. Inhibitory inputs: laminar inhibitory inputs made onto V1 excitatory cells of layers 2/3 through 6 (columns). LSPS evoked inputs are displayed as averaged inhibitory evoked inputs in units of pA and the percentage of inhibitory evoked input (%EI), which shows the relative contribution of synaptic input from each cortical layer to recorded cells. Average evoked inputs measured from each layer during the analysis window after photostimulation were compared with baseline spontaneous activity of 100 ms prior to photostimulation. Red values indicate non-significant laminar inputs inferred from such statistical comparisons ($P > 0.05$). Data are presented as the mean ± SE.

measured independent of EPSC strength (Fig. 4*B* and *D*), which provides a different means of evaluating excitatory synaptic connectivity across V1 laminar circuits.

L4 pyramidal neurons have a laminar input pattern distinguishable from L2/3 cells because they receive localized excitatory input mostly from L4 and L5a (Fig. 4 and Table 2). Although L4 cells receive some L2/3 input, they do not receive significant evoked input from L5b or L6 compared to baseline spontaneous activity. The EPSC input amplitudes from L5b and L6 during photostimulation do not differ significantly from those of spontaneously occurring EPSCs.

Among all the cortical cells in different laminar locations, L5 pyramidal cells have the most extensive input from the radial columns of laminar circuits and exhibit sublayer-specific connectivity to upper layer 5 (L5a) and lower layer 5 (L5b) pyramidal cells (Fig. 4 and Table 2). L5a and L5b are differentiated based upon cytoarchitectonic landmarks and cortical depths of the laminar positioning of the recorded cell somata. L5a pyramidal cells receive strong excitatory inputs from L2/3, L4 and L5a, and much weaker inputs from L5b and L6 (Table 2). In comparison, L5b pyramidal cells receive weak excitatory inputs from the radial columns with relatively concentrated inputs from L2/3 and L4 (Table 2). The average numbers of evoked EPSCs per photostimulation for L5a and L5b cells follow the trend of their laminar input amplitudes.

Compared with other cortical cells, L6 pyramidal cells receive generally weak and primarily localized inputs spanning a wide horizontal domain from within deep cortical layers (Fig. 4 and Table 2). L6 pyramidal neurons do not receive significant L2/3 input compared to baseline activity (Table 2).

Laminar inhibitory inputs to V1 excitatory neurons

Systematic examinations of inhibitory synaptic connectivity to excitatory neurons and comparisons of their excitatory connectivity indicate that the spatial distribution of local inhibitory inputs to V1 pyramidal neurons generally matches that of excitatory input sources for each cortical layer. The presence of inhibitory neurons in L1 prompted investigation of the extent of L1 inhibitory inputs to pyramidal neurons in L2/3, L4 and L5 because these cells have apical dendrites extended into L1 (Fig. 3). L2/3 pyramidal neurons receive a great majority of inhibitory inputs from L1, L2/3, L4 and L5a (Fig. 5 and Table 2). Compared to baseline spontaneous activity, L2/3 pyramidal neurons do not receive significant inhibitory input from L5b or L6, indicating a lack of direct inhibitory innervation from deep infragranular layers.

L4 pyramidal cells receive dominant inhibitory inputs from within L4 with some interlaminar inhibitory input from upper L5 (Fig. 5 and Table 2). L4 pyramidal neurons do not receive significant inhibitory inputs from L1, L2/3, L5b and L6. Notably, L4 received the fewest number of LSPS-evoked IPSCs compared to other layers (Fig. 5).

L5 excitatory pyramidal cells receive extensive inhibitory input from columnar circuits; these cells receive inhibitory input from both upper and deeper cortical layers (Fig. 5 and Table 2). Inhibitory inputs to L5b cells span the radial column of V1 with strongest input from within L5b (Fig. 5 and Table 2). LSPS-evoked inhibitory inputs to L5a or L5b cells from L1 are not statistically different from baseline activity. There is dense inhibitory innervation onto L5 pyramids from L5 and L6.

L6 pyramidal cells receive extensive inhibitory inputs from within L6 and slight inhibitory input from the upper cortical layers (Fig. 5 and Table 2). L1 and L2/3-evoked IPSCs measured in L6 pyramidal neurons are not statistically different from baseline activity.

Comparative excitatory and inhibitory laminar inputs across V1

To examine whether excitatory and inhibitory synaptic connectivity spatially overlaps, the spatial distributions of both excitatory and inhibitory synaptic input sources were compared for each layer across V1 laminar circuits. To directly compare excitatory and inhibitory input maps, aggregate synaptic input maps were normalized and coloured-coded on separate channels (Fig. 6*A* and *B*), and merged (Fig. 6*C*). Synaptic input fields of excitatory neurons span horizontally within laminar microcircuits, and cover 400–500 μm across the columnar microcircuits. To a large degree, excitatory neurons in each cortical layer appear to have matched excitatory and inhibitory synaptic input locations across both horizontal and vertical dimensions of columnar microcircuits. In validation of this balanced overlap, we further quantitatively compared the horizontal and vertical synaptic input profiles of excitatory and inhibitory synaptic connectivity (Fig. 6*D* and *E*). Statistical analyses indicate that the distributions of excitatory *vs.* inhibitory synaptic connectivity for excitatory neurons at a given layer do not differ significantly.

A separate analysis was used to measure the degree of matched spatial distribution of synaptic inputs across V1 laminar circuits. Average excitatory and inhibitory input maps were converted to binary matrices and synaptic inputs measured across the LSPS mapping grid were identified as either all or nothing per LSPS location. This method allowed direct evaluation of whether excitatory and inhibitory responses are either present or absent at a given spatial location. The number of matched pixels per group of neurons in distinct layers was then measured relative to the total locations surveyed by LSPS. The high degree of matched excitatory and inhibitory circuit topography across layers is found to be 81%,

95%, 89%, 82% and 81% for layers 2/3, 4, 5a, 5b and 6, respectively. This analysis reveals that pyramidal neurons receive closely matched distributions of excitatory and inhibitory connections across V1 laminar circuits.

Functional synaptic connectivity of mouse V1 laminar circuitry

Based upon our quantitative assessment of both excitatory and inhibitory synaptic laminar connections to excitatory

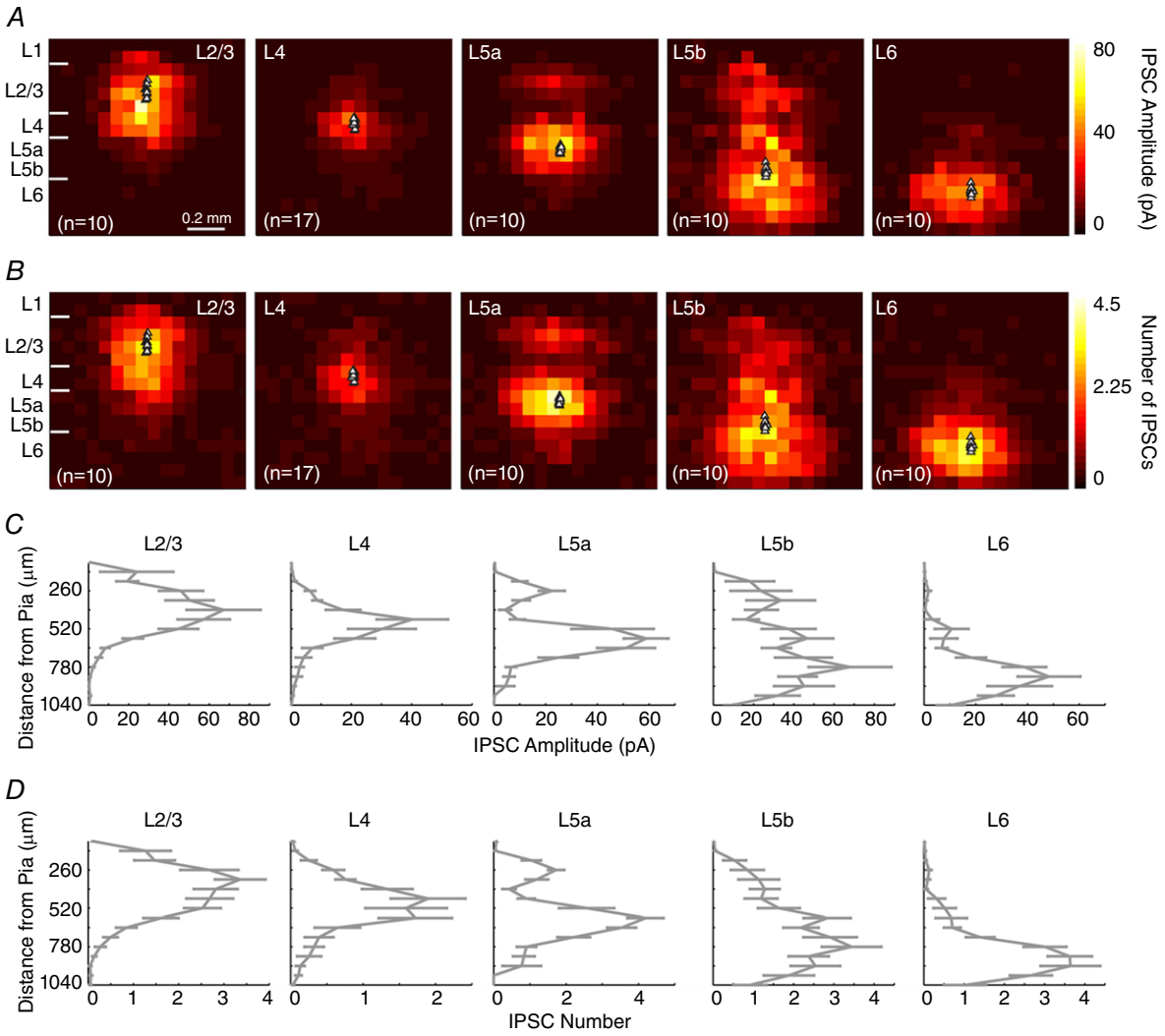

Figure 5. The spatial extent of local inhibitory inputs to V1 pyramidal neurons generally matches that of excitatory input sources for each cortical layer
A, group averaged inhibitory synaptic input maps for pyramidal neurons across V1 laminae. Each colour coded pixel represents the average IPSC amplitude across the LSPS mapping grid; black triangles represent the locations of recorded pyramidal neurons. The left most map charts V1 laminar boundaries relative to the LSPS mapping grid. *B*, numbers of IPSCs per LSPS location are plotted from the averaged maps presented in (*A*). For normalization, colour-coded laminar inhibitory input maps are scaled to the highest input value across groups. *C*, laminar profiles of evoked inhibitory synaptic input with average IPSC amplitudes quantified across the radial vector corresponding to the columnar position of recorded cells throughout the cortical depth. *D*, laminar profiles of evoked IPSC numbers quantified across the radial vector corresponding to the columnar position of recorded cells throughout the cortical depth, as in (*C*). Data are presented as the mean ± SE. The average numbers of evoked IPSCs per stimulation for L2/3 pyramidal cells are 0.6 ± 0.01, 2.6 ± 0.2, 2.6 ± 0.8 and 1.2 ± 0.7 for L1, L2/3, L4 and L5a, respectively (*B* and *D*). The average numbers of evoked IPSCs per stimulation for L4 pyramidal cells are 1.8 ± 0.6 and 1.18 ± 0.5 for L4 and L5a. The average numbers of evoked IPSCs per stimulation for L5a pyramidal cells are 1.1 ± 0.3, 1.7 ± 0.8, 3.9 ± 0.7, 2.2 ± 0.1 and 0.8 ± 0.2 from L2/3, L4, L5a, L5b and L6, respectively, whereas the values for L5b pyramidal cells are 1.0 ± 0.28, 1.5 ± 0.8, 2.4 ± 0.7, 2.8 ± 0.1 and 2.8 ± 0.2 from L2/3, L4, L5a, L5b and L6, respectively. The average numbers of evoked IPSCs per stimulation for L6 pyramidal cells are 0.4 ± 0.8, 0.7 ± 0.7, 1.4 ± 0.1 and 3.4 ± 0.2 from L4, L5a, L5b and L6, respectively.

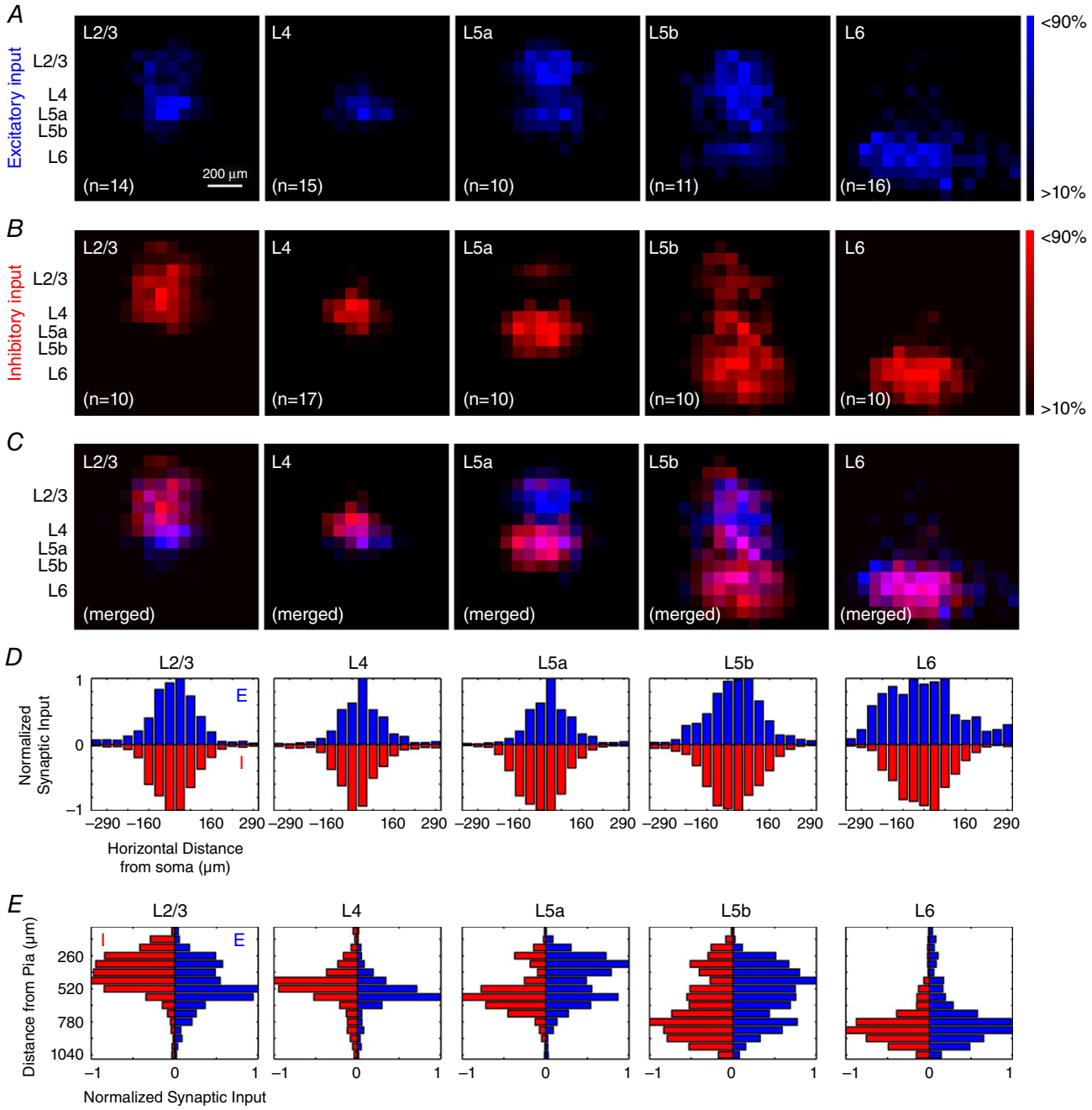

Figure 6. Excitatory and inhibitory synaptic connectivity spatially overlap in a balanced manner for each layer across V1 circuits

A, excitatory synaptic input maps are normalized within respective postsynaptic layers and re-plotted from black to blue. Dominant local pathways are displayed by filtering the lower 10% of excitatory inputs based upon EPSC amplitude and scaling the respective laminar maps to 90% of the largest excitatory synaptic inputs measured. *B*, inhibitory synaptic input maps are normalized within respective postsynaptic layers and plotted across lamina, as in (*A*) but colour coded from black to red. Consistent with (*A*), dominant local pathways are displayed from filtering the lower 10% of excitatory inputs based upon IPSC amplitude and scaling the respective maps to 90% of the largest inhibitory synaptic inputs measured within respective postsynaptic layers. *C*, excitatory and inhibitory normalized input maps are merged according to the laminar position of recorded postsynaptic neurons; violet pixels represent locations of matched synaptic input from both presynaptic excitatory and inhibitory input domains. *D*, horizontal distribution of normalized excitatory inputs (blue) and inhibitory inputs (red) are plotted for inputs measured across the vertical vector on the LSPS mapping grid to the recorded postsynaptic neurons. *E*, vertical distribution of normalized synaptic inputs are plotted for inputs measured across the horizontal vector on the LSPS mapping grid to the recorded postsynaptic neurons.

cells in each cortical layer, we constructed layer-by-layer synaptic wiring diagrams indicating the comparative strength of excitatory and inhibitory inputs to excitatory neurons in the visual cortex (Fig. 7). Using the quantitative data shown in Table 2, the average excitatory and inhibitory input strength of specific cortical laminae to targeted postsynaptic excitatory cells was visualized in the matrices of Fig. 7*A* and *B*, respectively. Several features merged from functional wiring diagrams of excitatory neurons are summarized in Fig. 7*C* for which matched excitatory and inhibitory circuit topography is clearly seen.

The strength of excitatory and inhibitory connections to L2/3, L4 and L5a pyramidal cells exceeded the connection strength of L5b and L6 pyramids. Although strong interlaminar excitatory connections are known to exist between excitatory cells (e.g. L4 → L2/3; L2/3 ↔ L5), in the present study, we unravelled robust interlaminar inhibitory inputs to these excitatory neurons, which indicates that inhibitory cortical connections are not necessarily limited in highly localized dimensions as generally described (Binzegger *et al.* 2004; Thomson & Lamy, 2007; Katzel *et al.* 2011). In addition, L4 and L5a excitatory cells have stronger intralaminar excitatory connections than L2/3, L5b and L6 cells; L4 cells, which comprise the major thalamocortical input layer, have weaker intralaminar inhibitory connections than the cells in other cortical layers. Only L2/3 cells have significant inhibitory input from L1.

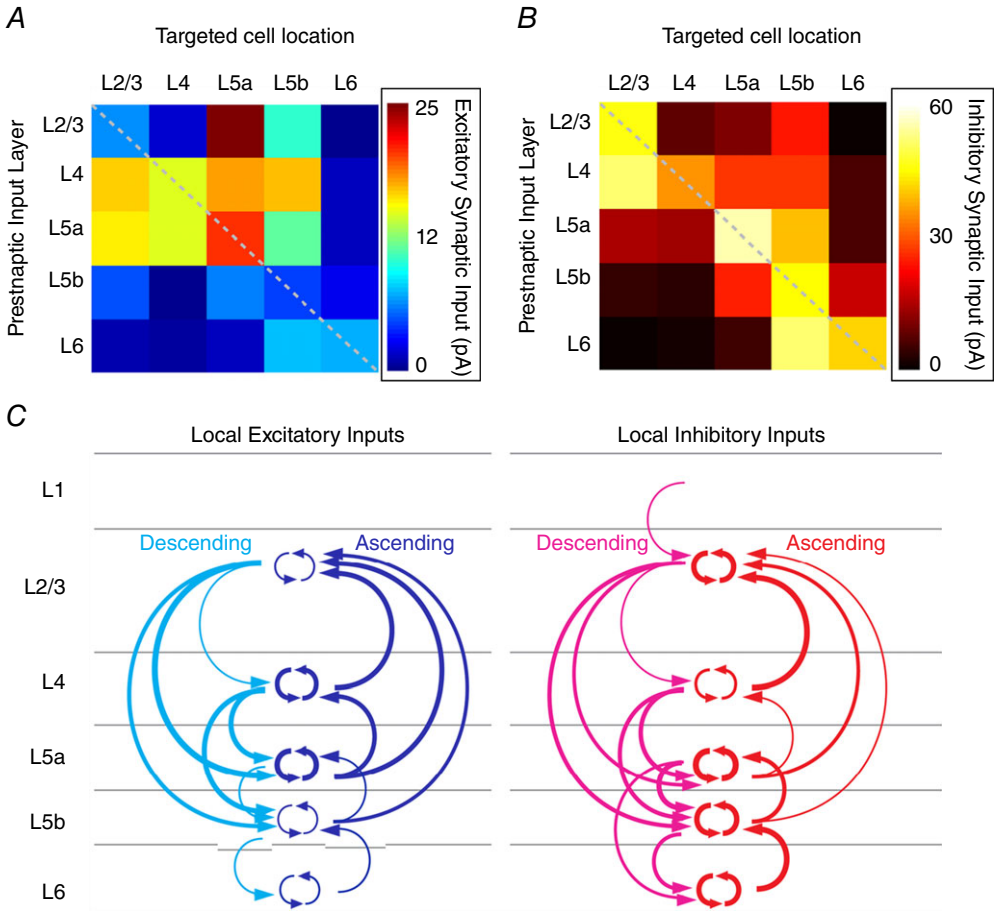

Figure 7. Organization of the comparative strength of excitatory and inhibitory inputs between cortical layers in local V1 circuits
A, input layer → single neuron connectivity matrix showing average excitatory inputs from specific cortical laminae to targeted postsynaptic pyramidal cells (for detailed quantitative results, see Table 2). *B*, input layer → single neuron connectivity matrix showing average inhibitory inputs from specific cortical laminae to targeted postsynaptic pyramidal cells (for detailed quantitative results, see Table 2). *C*, functional wiring diagram of excitatory neurons constructed based upon the quantitative assessments shown in (*A*) and (*B*). Left: excitatory laminar inputs to pyramidal cells across V1 local circuits. Descending interlaminar excitatory inputs are indicated in cyan and ascending interlaminar excitatory inputs are indicated in blue. Intralaminar inputs are shown within each targeted layer. Note that the thickness of arrows indicates the relative strength of synaptic connectivity from the input layer to the recipient neurons. Right: inhibitory laminar inputs to pyramidal cells. Descending interlaminar inhibitory inputs are indicated in violet and ascending interlaminar inhibitory inputs are indicated in red.

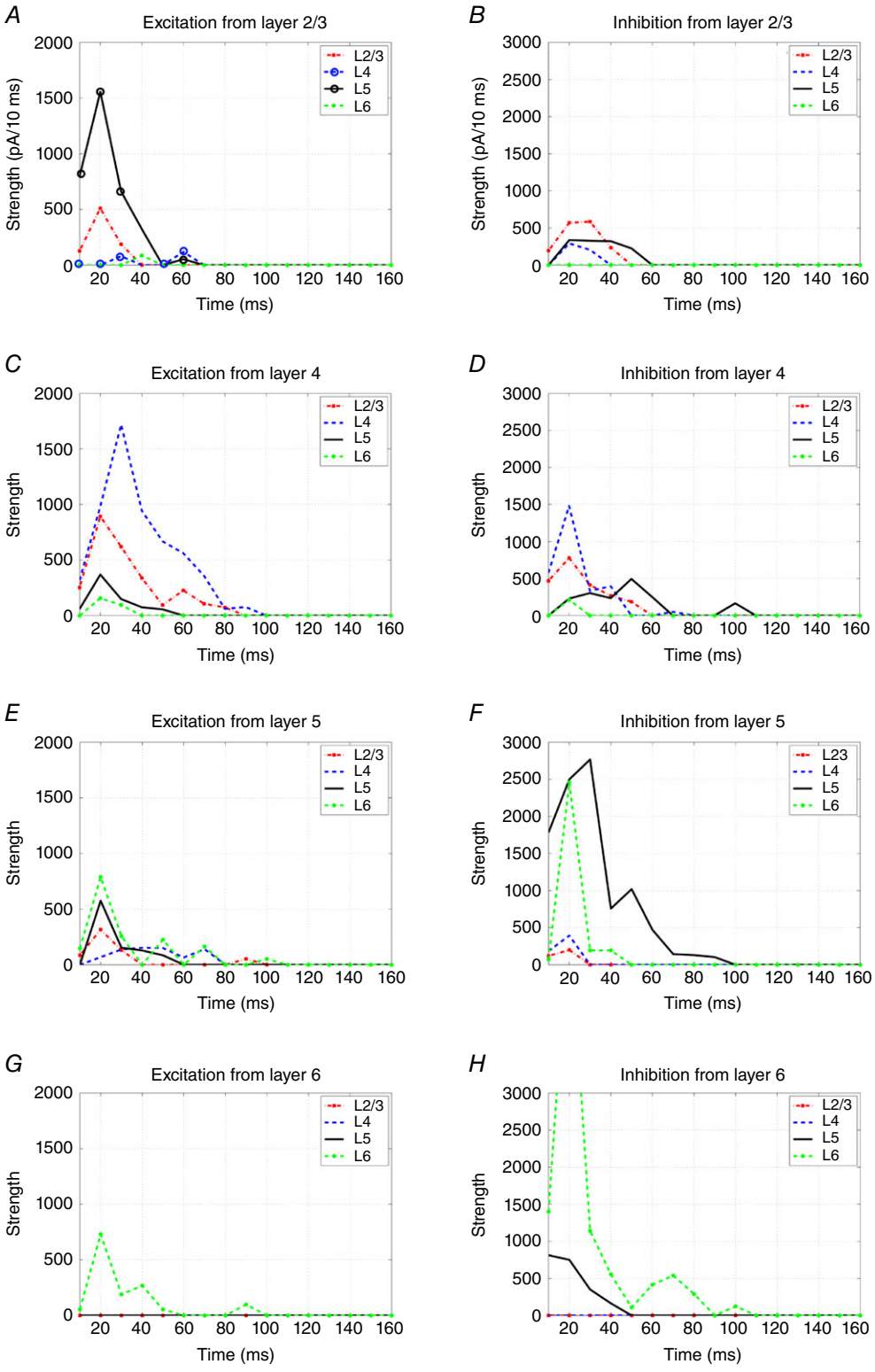

Figure 8. The temporal evolution and laminar distributions of local V1 circuit inputs to excitatory pyramidal neurons across different cortical layers in response to layer-specific photostimulation
A, *C*, *E* and *G*, each showing excitatory inputs to L2/3, L4, L5 and L6 excitatory neurons in response to photostimulation in L2/3, L4, L5 and L6, respectively. *B*, *D*, *F* and *H*, each showing inhibitory inputs to L2/3, L4, L5 and L6 excitatory neurons in response to photostimulation in L2/3, L4, L5 and L6, respectively. The *x*-axis represents the time (ms) and the *y*-axis represents the input strength (integrated synaptic input strength, pA/10 ms). Lines with different colours indicate the plots of inputs to the specified cortical layers.

In addition, we examined the temporal features of laminar distributions of local V1 circuit inputs to excitatory pyramidal neurons. To complement the static wiring (Fig. 7), the temporal evolution of excitatory and inhibitory synaptic inputs to excitatory neurons in different cortical layers is shown in Fig. 8. Based on the data derived from a typical subset of sampled neurons, a great majority of inputs are observed to occur within 100 ms of layer-specific photostimulation, with the peak input strengths located between 20 and 40 ms. In Fig. 8*A*, the L5 excitation in response to L2/3 photostimulation exhibits a single peak that is temporally correlated with the L2/3 excitation, and the L2/3 → L5 input quickly falls off to the baseline at ∼50 ms post-photostimulation. If there were significant polysynaptic activation, the L5 excitation should have been broader with multiple peaks, and the L4 excitation would be much stronger. In Fig. 8*C*, L4 → L2/3 or L5 excitation peaks earlier than the L4 excitation. Their excitation falls rapidly, as predicted by the time course of the direct inputs. In addition, layer-specific inhibition generally decays quickly (Fig. 8*B*, *D*, *F* and *H*), matching the time course of layer-restricted excitation (Fig. 8*A*, *C*, *E* and *G*). Taken together, this temporal analysis supports the conclusion that LSPS maps direct synaptic inputs, and argues strongly against the possibility that feed-forward synaptically driven events could account for most of the input mapping responses measured.

A discrete dynamical model (Christley *et al.* 2009) was used to infer the connectivity among excitatory neurons at four different cortical layers. As shown in Fig. 9, the photostimulation-evoked circuit input activities are simulated well by the discrete dynamical model. The model simulations further support that the temporal evolution of excitatory and inhibitory synaptic inputs to excitatory neurons is laminar-specific and balanced in the visual cortex. The proof-of-principle demonstration indicates that our photostimulation-based experiments are capable of generating effective spatiotemporal data that can be directly used through computational modelling to predict the cortical circuit operations.

Discussion

In the present study, we have used the LSPS mapping approach to assess connectivity of excitatory cells → excitatory cells and inhibitory cells → excitatory cells on a layer-by-layer basis in local mouse V1 circuitry. The comprehensive and quantitative analysis allows for the construction of precise synaptic wiring diagrams of excitatory neurons in the visual cortex, which demonstrates the preserved excitatory laminar connectivity features reported previously in mouse primary somatosensory (S1), secondary somatosensory (S2) and primary motor cortex (M1) (Weiler *et al.* 2008; Hooks *et al.* 2011). This finding is consistent with the general notion that cortical organization provides a common computation platform with shared features between different cortical areas. We show that excitatory and inhibitory synaptic connectivity in V1 is spatially balanced across excitatory neuronal networks for all cortical layers, which is striking when considering that excitatory cells greatly outnumber the inhibitory cells in the cortex. The present study also provides a high resolution map of local V1 inhibitory circuit connections.

Until now, the synaptic organization of V1 excitatory neurons has not been examined comprehensively across all cortical layers at single cell resolution using LSPS, as in S1, S2 and M1 (Shepherd & Svoboda, 2005; Weiler *et al.* 2008; Hooks *et al.* 2011). Although we have mapped inter-laminar functional connectivity and circuit dynamics at the neuronal population level in mouse V1 through fast voltage-sensitive dye imaging and photostimulation (Xu *et al.* 2010*b*; Olivas *et al.* 2012), the published studies have limitations in that voltage-sensitive dye imaging does not have a single cell resolution and do noy allow us to map circuit inhibition independently. Because detailed anatomical studies do not address the magnitude of functional synaptic connections (Burkhalter, 1989; Binzegger *et al.* 2004) and paired intracellular recordings only provide limited circuit connectivity profiles at a microscopic level, the present study complements our previous imaging studies with mapping local circuit connections to single neurons located in specific V1 layers with LSPS and whole cell recordings.

Although both excitatory cell subtypes, spiny stellates and pyramidal cells, have been reported in layer 4 of monkey and cat V1 (Lund *et al.* 1979; Saint Marie & Peters, 1985; Anderson *et al.* 1994; Stratford *et al.* 1996), as well as in rat and mouse S1 (Schubert *et al.* 2003; Feldmeyer *et al.* 2005), almost all the recorded L4 cells in our sample were morphologically identified as pyramidal with apical dendrites spanning to the pial surface, as also reported in guinea-pig V1 L4 excitatory cells (Saez & Friedlander, 2009). This is probably a result of whole-cell recording selection bias partly attributed to the use of DIC aided visualization. The excitatory laminar connectivity of mouse V1 circuits shares some common features with other cortical regions, including mouse and rat primary somatosensory, mouse secondary somatosensory, and mouse primary motor cortex and primary auditory cortex (A1) (Shepherd & Svoboda, 2005; Weiler *et al.* 2008; Hooks *et al.* 2011). Note that these previous studies did not map inhibitory connections. Strong excitatory connections include the L4 projections to L2/3 and L5 and the reciprocal projections between L2/3 and L5. L2/3 excitatory cells receiving strong projections from L4 and L5a have also been demonstrated in S1 and A1 of the rat and mouse (Shepherd & Svoboda, 2005; Xu & Callaway, 2009; Oviedo *et al.* 2010). In terms of local cortical connectivity, mouse V1 L4 pyramidal cells receive

dominant inputs from L4 and L5a but with some input from L2/3, differing from rat S1 L4 spiny stellate cells that have circuit connections almost exclusively from within the same barrel in L4 (Schubert *et al.* 2003). In mouse V1, there are sublayer-specific connections with L5 pyramidal cells where inputs from L2/3→L5a are stronger than L2/3→L5b, generally similar to that observed in mouse motor and somatosensory regions (Anderson *et al.* 2010; Hooks *et al.* 2011). Note that Anderson *et al.* (2010) further showed pathway-specific L2/3 → L5b projections because L2/3 inputs to L5B corticospinal neurons are very robust but L2/3 inputs to L5B corticostriatal neurons are significantly less so. However, in the present study, we found that L5 excitatory pyramidal cells have extensive excitatory connections throughout the cortical columns (L2/3–L6), which appears to be different from mouse S1 (Hooks *et al.* 2011; but see rat S1 in Schubert *et al.* 2001) and mouse M1 (Weiler *et al.* 2008; Anderson *et al.* 2010), but more similar to L5 neurons in monkey V1 (Briggs & Callaway, 2005). This suggests that L5 cells functionally integrate information from a broad range of V1 circuit connections. L6 interlaminar input and output connections are weak, as seen in rat V1 (Zarrinpar & Callaway, 2006) and in mouse motor and somatosensory areas (Hooks *et al.* 2011). The absence of L6 → L4 connectivity as inferred from ascending L6 axonal projections to L4 in highly visual mammals, such as cats and monkeys, may represent a species-specific feature not found in rodents. This potential species difference suggests that there may be L6 projections to non-excitatory cells in rodent L4 that have not yet been examined thoroughly.

Compared with connectivity of excitatory cells → excitatory cells, inhibitory synaptic connections across V1 laminar circuitry are much less understood (Thomson & Lamy, 2007). Although cell-type specificity has emerged as a common feature of microcortical connections, recent studies highlight a high density of promiscuous, unspecific inhibitory connectivity onto excitatory neurons, which can provide a global 'blanket of inhibition' to nearby excitatory neurons (Fino & Yuste, 2011; Packer & Yuste, 2011; Fino *et al.* 2013; Packer *et al.* 2013). Whether specific inhibitory neurons are wired specifically in different scales of cortical circuits remains to be investigated (Otsuka & Kawaguchi, 2009). The present study has provided new information on inhibitory synaptic connections to excitatory neurons on a layer-by-layer basis across local cortical circuitry and indicates that the laminar organization of inhibitory inputs is more specific than previously assumed. In addition, the prominent interlaminar inhibitory connections (as seen in L4 → L2/3, between

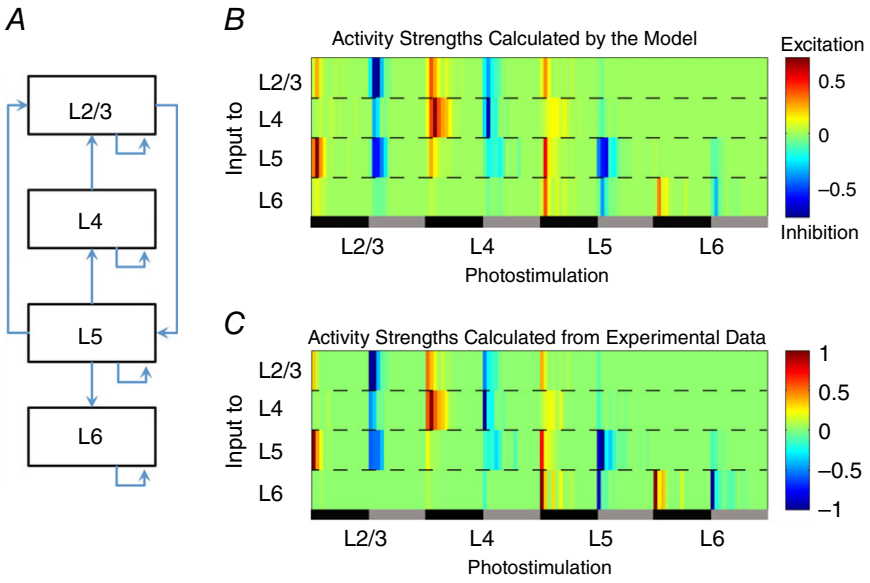

Figure 9. Photostimulation mapped circuit activities are simulated by the discrete dynamical model
A simplified laminar connectivity map (*A*) and the temporal evolution data across layers are used for the prior information in the model. *B*, synaptic input strengths at given time points in different cortical layers simulated by the discrete dynamical model with the optimal connectivity matrix (see Methods) [0.7818, −0.04, −0.0049, 0; 0, 0.6933, 0.0129, 0; 0.2200, 0, 0.6087, 0; 0, 0, 0.1086, 0.3108]. *C*, synaptic input strengths at given time points in different layers observed by experiments. The *x*-axis of (*B*) and (*C*) represents the conditions of photostimulation in L2/3, L4, L5 and L6. For each photostimulation in a specified layer, the dark zone indicates the temporal domain (150 ms post-photostimulation) of excitatory inputs evoked by photostimulation, whereas the grey zone indicates the temporal domain (150 ms post-photostimulation) of inhibitory inputs. The *y*-axis of (*B*) and (*C*) represents the input strengths for L2/3, L4, L5 and L6, according to the colour scales, in which the relative activation strengths are coded at given time points.

L2/3 and L5, L6 → L5) can help to explain V1 circuit interaction and physiology both *in vitro* and *in vivo* (Olsen *et al.* 2012).

Laminar inhibitory connections to excitatory cells in primary motor, somatosensory and visual cortex have been examined using genetically targeted photostimulation in a mouse knock-in line that conditionally expresses channelrhodopsin-2 in GABAergic neurons (Katzel *et al.* 2011). Despite technical considerations concerning varied channelrhodopsin-2 expression levels in inhibitory neurons and partial targeting of all inhibitory cells, Katzel *et al.* (2011) reported that inhibitory inputs to excitatory neurons derive largely from the same cortical layer, with subsets of pyramidal cells in layers 2/3 and 5B receiving extensive interlaminar inhibition. As a result of the established robustness of glutamate uncaging, the present study shows more extensive interlaminar inhibitory circuit connections to excitatory neurons in all cortical layers in addition to intralaminar inhibitory connections. The LSPS approach can effectively map the overall inhibitory connections from diverse inhibitory cell types to targeted cell types, although it is not possible to clarify the specific contributions of precise inhibitory cell types with respect to the total inhibitory synaptic input to the recorded neurons because glutamate uncaging activates different types of inhibitory neurons agnostically.

Thus, although it is important to examine overall inhibitory inputs first using LSPS, we plan to map cell type-specific inhibitory connections using optogenetic methods that genetically target and selectively photoactivate specific subsets of inhibitory cortical neurons providing inputs to excitatory neurons. Clearly, the cell-type specific input mapping study will require a large investment of our effort to extend the present fundamental findings described in the present study.

On the basis of the functional circuit mapping, the present study has provided important information for further computational modelling analysis. In particular, through *in silico* perturbation of circuit nodes in the model, dynamic network characteristics beyond the direct laminar circuit connections may be obtained. For example, an early initiating event in visual critical period plasticity is disinhibition in L2/3. One day of monocular deprivation during the critical period reduces excitatory drive onto parvalbumin-positive interneurons in binocular V1. This decrease in cortical inhibition is permissive for synaptic competition between excitatory inputs from each eye and is sufficient for subsequent shifts in excitatory neuronal ocular dominance (Kuhlman *et al.* 2013). Although the impact in L2/3 has been directly assessed, whether the effects of disinhibition may be expanded to other cortical layers remains to be explored. To address this and other related questions, we aim to test the circuit model in the future by blocking inhibitory projections from L2/3 inhibitory neurons to excitatory neurons. Reciprocally, physiological mapping experiments can be designed to test the predictions made by the model. Given that L2/3 neurons send strong projections to L5, we predict that the disinhibition effect would propagate to L5 for the laminar shift of cortical plasticity. Taken together, the interplay between modelling and experiment will probably provide new insights that could not be obtained by the experimental approach alone because the model drives the experimental design.

References

Anderson CT, Sheets PL, Kiritani T & Shepherd GM (2010). Sublayer-specific microcircuits of corticospinal and corticostriatal neurons in motor cortex. *Nat Neurosci* **13**, 739–744.

Anderson JC, Douglas RJ, Martin KA & Nelson JC (1994). Synaptic output of physiologically identified spiny stellate neurons in cat visual cortex. *J Comp Neurol* **341**, 16–24.

Antonini A, Fagiolini M & Stryker MP (1999). Anatomical correlates of functional plasticity in mouse visual cortex. *J Neurosci* **19**, 4388–4406.

Apicella AJ, Wickersham IR, Seung HS & Shepherd GM (2012). Laminarly orthogonal excitation of fast-spiking and low-threshold-spiking interneurons in mouse motor cortex. *J Neurosci* **32**, 7021–7033.

Binzegger T, Douglas RJ & Martin KA (2004). A quantitative map of the circuit of cat primary visual cortex. *J Neurosci* **24**, 8441–8453.

Briggs F & Callaway EM (2005). Laminar patterns of local excitatory input to layer 5 neurons in macaque primary visual cortex. *Cereb Cortex* **15**, 479–488.

Burkhalter A (1989). Intrinsic connections of rat primary visual cortex: laminar organization of axonal projections. *J Comp Neurol* **279**, 171–186.

Callaway EM (1998). Local circuits in primary visual cortex of the macaque monkey. *Annu Rev Neurosci* **21**, 47–74.

Chattopadhyaya B, Di Cristo G, Higashiyama H, Knott GW, Kuhlman SJ, Welker E & Huang ZJ (2004). Experience and activity-dependent maturation of perisomatic GABAergic innervation in primary visual cortex during a postnatal critical period. *J Neurosci* **24**, 9598–9611.

Christley S, Nie Q & Xie X (2009). Incorporating existing network information into gene network inference. *PLoS ONE* **4**, e6799.

D'Amour JA & Froemke RC (2015). Inhibitory and excitatory spike-timing-dependent plasticity in the auditory cortex. *Neuron* **86**, 514–528.

Dantzker JL & Callaway EM (2000). Laminar sources of synaptic input to cortical inhibitory interneurons and pyramidal neurons. *Nat Neurosci* **3**, 701–707.

Douglas RJ & Martin KA (2004). Neuronal circuits of the neocortex. *Annu Rev Neurosci* **27**, 419–451.

Feldmeyer D, Roth A & Sakmann B (2005). Monosynaptic connections between pairs of spiny stellate cells in layer 4 and pyramidal cells in layer 5A indicate that lemniscal and paralemniscal afferent pathways converge in the infragranular somatosensory cortex. *J Neurosci* **25**, 3423–3431.

Fino E, Packer AM & Yuste R (2013). The logic of inhibitory connectivity in the neocortex. *Neuroscientist* **19**, 228–237.

Fino E & Yuste R (2011). Dense inhibitory connectivity in neocortex. *Neuron* **69**, 1188–1203.

Haider B, Hausser M & Carandini M (2013). Inhibition dominates sensory responses in the awake cortex. *Nature* **493**, 97–100.

Harris KD & Shepherd GM (2015). The neocortical circuit: themes and variations. *Nat Neurosci* **18**, 170–181.

Hasenstaub A, Shu Y, Haider B, Kraushaar U, Duque A & McCormick DA (2005). Inhibitory postsynaptic potentials carry synchronized frequency information in active cortical networks. *Neuron* **47**, 423–435.

Hooks BM, Hires SA, Zhang YX, Huber D, Petreanu L, Svoboda K & Shepherd GM (2011). Laminar analysis of excitatory local circuits in vibrissal motor and sensory cortical areas. *PLoS Biol* **9**, e1000572.

Ikrar T, Olivas ND, Shi Y & Xu X (2011). Mapping inhibitory neuronal circuits by laser scanning photostimulation. *J Vis Exp* **56**, 3109.

Ikrar T, Shi Y, Velasquez T, Goulding M & Xu X (2012). Cell-type specific regulation of cortical excitability through the allatostatin receptor system. *Front Neural Circuits* **6**, 2.

Kapfer C, Glickfeld LL, Atallah BV & Scanziani M (2007). Supralinear increase of recurrent inhibition during sparse activity in the somatosensory cortex. *Nat Neurosci* **10**, 743–753.

Katzel D, Zemelman BV, Buetfering C, Wolfel M & Miesenbock G (2010). The columnar and laminar organization of inhibitory connections to neocortical excitatory cells. *Nat Neurosci* **14**, 100–107.

Katzel D, Zemelman BV, Buetfering C, Wolfel M & Miesenbock G (2011). The columnar and laminar organization of inhibitory connections to neocortical excitatory cells. *Nat Neurosci* **14**, 100–107.

Kuhlman SJ, Olivas ND, Tring E, Ikrar T, Xu X & Trachtenberg JT (2013). A disinhibitory microcircuit initiates critical-period plasticity in the visual cortex. *Nature* **501**, 543–546.

Lund JS, Henry GH, MacQueen CL & Harvey AR (1979). Anatomical organization of the primary visual cortex (area 17) of the cat. A comparison with area 17 of the macaque monkey. *J Comp Neurol* **184**, 599–618.

Markram H, Toledo-Rodriguez M, Wang Y, Gupta A, Silberberg G & Wu C (2004). Interneurons of the neocortical inhibitory system. *Nat Rev Neurosci* **5**, 793–807.

Oliva AA, Jr., Jiang M, Lam T, Smith KL & Swann JW (2000). Novel hippocampal interneuronal subtypes identified using transgenic mice that express green fluorescent protein in GABAergic interneurons. *J Neurosci* **20**, 3354–3368.

Olivas ND, Quintanar-Zilinskas V, Nenadic Z & Xu X (2012). Laminar circuit organization and response modulation in mouse visual cortex. *Front Neural Circuits* **6**, 70.

Olsen SR, Bortone DS, Adesnik H & Scanziani M (2012). Gain control by layer six in cortical circuits of vision. *Nature* **483**, 47–52.

Otsuka T & Kawaguchi Y (2009). Cortical inhibitory cell types differentially form intralaminar and interlaminar subnetworks with excitatory neurons. *J Neurosci* **29**, 10533–10540.

Oviedo HV, Bureau I, Svoboda K & Zador AM (2010). The functional asymmetry of auditory cortex is reflected in the organization of local cortical circuits. *Nat Neurosci* **13**, 1413–1420.

Packer AM, McConnell DJ, Fino E & Yuste R (2013). Axo-dendritic overlap and laminar projection can explain interneuron connectivity to pyramidal cells. *Cereb Cortex* **23**, 2790–2802.

Packer AM & Yuste R (2011). Dense, unspecific connectivity of neocortical parvalbumin-positive interneurons: a canonical microcircuit for inhibition? *J Neurosci* **31**, 13260–13271.

Pluta S, Naka A, Veit J, Telian G, Yao L, Hakim R, Taylor D & Adesnik H (2015). A direct translaminar inhibitory circuit tunes cortical output. *Nat Neurosci*.

Saez I & Friedlander MJ (2009). Synaptic output of individual layer 4 neurons in guinea pig visual cortex. *J Neurosci* **29**, 4930–4944.

Saint Marie RL & Peters A (1985). The morphology and synaptic connections of spiny stellate neurons in monkey visual cortex (area 17): a Golgi-electron microscopic study. *J Comp Neurol* **233**, 213–235.

Schubert D, Kotter R, Zilles K, Luhmann HJ & Staiger JF (2003). Cell type-specific circuits of cortical layer IV spiny neurons. *J Neurosci* **23**, 2961–2970.

Schubert D, Staiger JF, Cho N, Kotter R, Zilles K & Luhmann HJ (2001). Layer-specific intracolumnar and transcolumnar functional connectivity of layer V pyramidal cells in rat barrel cortex. *J Neurosci* **21**, 3580–3592.

Shepherd GM, Pologruto TA & Svoboda K (2003). Circuit analysis of experience-dependent plasticity in the developing rat barrel cortex. *Neuron* **38**, 277–289.

Shepherd GM & Svoboda K (2005). Laminar and columnar organization of ascending excitatory projections to layer 2/3 pyramidal neurons in rat barrel cortex. *J Neurosci* **25**, 5670–5679.

Shi Y, Nenadic Z & Xu X (2010). Novel use of matched filtering for synaptic event detection and extraction. *PLoS ONE* **5**, e15517.

Silberberg G & Markram H (2007). Disynaptic inhibition between neocortical pyramidal cells mediated by Martinotti cells. *Neuron* **53**, 735–746.

Stratford KJ, Tarczy-Hornoch K, Martin KA, Bannister NJ & Jack JJ (1996). Excitatory synaptic inputs to spiny stellate cells in cat visual cortex. *Nature* **382**, 258–261.

Thomson AM & Lamy C (2007). Functional maps of neocortical local circuitry. *Front Neurosci* **1**, 19–42.

Weiler N, Wood L, Yu J, Solla SA & Shepherd GM (2008). Top-down laminar organization of the excitatory network in motor cortex. *Nat Neurosci* **11**, 360–366.

Xu X & Callaway EM (2009). Laminar specificity of functional input to distinct types of inhibitory cortical neurons. *J Neurosci* **29**, 70–85.

Xu X, Roby KD & Callaway EM (2010*a*). Immunochemical characterization of inhibitory mouse cortical neurons: three chemically distinct classes of inhibitory cells. *J Comp Neurol* **518**, 389–404.

Xu X, Olivas ND, Levi R, Ikrar T & Nenadic Z (2010*b*). High precision and fast functional mapping of cortical circuitry through a combination of voltage sensitive dye imaging and laser scanning photostimulation. *J Neurophysiol* **103**, 2301–2312.

Xu X, Roby KD & Callaway EM (2006). Mouse cortical inhibitory neuron type that coexpresses somatostatin and calretinin. *J Comp Neurol* **499**, 144–160.

Yoshimura Y, Dantzker JL & Callaway EM (2005). Excitatory cortical neurons form fine-scale functional networks. *Nature* **433**, 868–873.

Zarrinpar A & Callaway EM (2006). Local connections to specific types of layer 6 neurons in the rat visual cortex. *J Neurophysiol* **95**, 1751–1761.

Additional information

Competing interests

The authors declare that they have no competing interests.

Funding

This work was funded by the US National Institutes of Health (NIH) grants NS078434 and MH105427 to XX. The computational analysis work was supported by a seed fund from the NIH Center of Excellence Grant P50GM76516. QN was partially supported by National Science Foundation grant DMS-1161621, and NIH grants R01GM107264, R01NS095355, R01ED023050.

Author contributions

NDO, TI and TP conducted the electrophysiological experiments and computational analysis. NDO, TP, YS, QN, MF and XX performed data analysis. XX designed the project, wrote the manuscript and completed the revisions. All authors declare that they have no conflicts of interest. All authors have approved the final version of the manuscript and agree to be accountable for all aspects of the work. All persons designated as authors qualify for authorship, and all those who qualify for authorship are listed.